Supporting Information

Electrical Double Layer of Supported Atomically-thin Materials

Sun Sang Kwon,[†,∥] Jonghyun Choi,[‡,∥] Mohammad Heiranian,[‡] Yerim Kim,[‡] Won Jun Chang,[†] Peter M. Knapp,[‡] Michael Cai Wang,[‡] Jin Myung Kim,[§] Narayana R. Aluru,[‡] Won Il Park,[,†] and SungWoo Nam[*,‡,§]*

[†]Division of Materials Science and Engineering, Hanyang University, Seoul 04763, Korea

[‡]Department of Mechanical Science and Engineering, University of Illinois at Urbana-Champaign, Urbana, Illinois 61801, United States

[§]Department of Materials Science and Engineering, University of Illinois at Urbana-Champaign, Urbana, Illinois 61801, United States

[∥]These authors contributed equally to this work.

[*]Correspondence and requests for materials should be addressed to W.I.P. (email: wipark@hanyang.ac.kr) or to S.N. (email: swnam@illinois.edu)

Measurements of wettability

A CAM200 goniometer (KSV Instruments Ltd., Helsinki, Finland) on a vibration-isolated table was used for macroscopic measurement of water contact angles (WCAs) (Figure S1). Identical volume droplets of five microliters were used for all experiments for consistency. A high-speed camera was used to capture the droplet images during measurements, and the static WCAs were determined within 3 seconds of the droplet reaching the sample. The WCA was calculated based on the Young-Laplace equation using the software.[1,2] For the measurement of microscopic WCAs (Figure S2), a FEI Quanta FEG 450 environmental scanning electron microscope (E-SEM) was used for water droplet condensation with a Peltier cooler temperature of 4 ºC and a chamber pressure of 6.2 torr. Lower temperatures (2.5 – 3.0 ºC) were used for water droplet condensation on thermally insulating substrates (e.g., graphene on polyethylene terephthalate (PET) and polyimide (PI)). The contact angle measurements were performed based on the Young-Laplace equation using ImageJ software (NIH, USA) operating on the E-SEM images.[1–3] The measured WCAs were considered as valid only if the droplets did not induce delamination of graphene (checked by evaporating the droplets by decreasing the chamber pressure). At least five condensed spherical droplets were analyzed for each condition.

Calculation of capacitance from cyclic voltammetry

In cyclic voltammetry (CV) measurements (Figure S3), the measured area inside the potential window between the anodic and cathodic sweep curves is directly proportional to the capacitance, which is calculated as follows:

$$C_T = \frac{S_2 - S_1}{2v(E_2 - E_1)} \quad (2)$$

Here, S_2-S_1 denotes the area of the potential window, v is the voltage sweep rate, E_2 and E_1 are the two endpoints of the voltage sweep range (-0.3 and +0.7 V), respectively.

Calculation of quantum capacitance and EDL capacitance

The quantum capacitance (C_Q) of graphene was calculated to estimate the EDL capacitance (C_{EDL}) from the measured total capacitance (C_T) [4,5] (Figure S5a):

$$C_Q = \frac{2e^2 k_B T}{\pi(\hbar v_F)^2} \ln[2(1+\cosh\frac{eV}{k_B T})] \quad (1)$$

where $\hbar$ is the reduced Planck constant, e is the elementary charge, k_B is the Boltzmann constant, T is the temperature, $v_F \approx$ c/300 is the Fermi velocity of the Dirac electron, and $V = E_F/e$ is the potential of graphene. Figure S5b shows the C_{EDL} as a function of the applied gate bias. The C_{EDL} exhibits characteristics similar to C_T, where the minimum capacitance and gate modulation level were both suppressed for graphene supported on a hydrophobic substrate.

Computational Methods

Molecular dynamics simulations (MD) were performed using the LAMMPS package.[6] The systems were generated using Visual Molecular Dynamics (VMD).[7] To study the effect of the hydrophilicity on the EDL near graphene, two simulation boxes with different substrates were set up. In the first simulation, the substrate was SiO_2, and the second substrate was PTFE-coated SiO_2.

As shown in Figure S6, each simulation box consisted of a single-layer graphene sheet, the substrate (PTFE/SiO_2 and SiO_2), water, and ions. The two systems (containing ~15,000 atoms) had dimensions of 5 nm x 5 nm x 10 nm. Periodic boundary conditions were applied in all three directions. The Lennard-Jones (LJ) potential with a cutoff distance of 1.2 nm was employed to model the non-bonded interactions. The long–range electrostatic interactions were computed using particle-particle particle-mesh (PPPM).[8] An extended simple point charge (SPC/E) water model with the SHAKE algorithm was used. The SHAKE algorithm maintains the rigidity of each water molecule. Water was ionized by 1M potassium chloride. The LJ parameters for the ions are given in ref 9. The graphene and substrate atoms were fixed in space; therefore, only their interactions with water and ions were considered. The LJ parameters for graphene, SiO_2, and PTFE were obtained from the force fields developed by Wu et al.,[10] Cygan et al.[11] and Daly et al.,[12] respectively.

The energy of each system was minimized for 10,000 steps before the simulations. The simulation were then performed in an NPT (i.e., constant number of particles, constant pressure and constant temperature) ensemble for 5 ns at a pressure of 1 atm and a temperature of 300 K until the water reached its equilibrium density. No external force was applied in the simulations. Temperature was maintained at 300 K by using the Nosè-Hoover thermostat[13,14] with a time constant of 0.1 ps. The production simulations were performed in an NVT (i.e., constant number of particles, constant volume and constant temperature) ensemble for 5 ns at the same pressure and temperature. Trajectories of ions were dumped every picosecond to study the structure of ions near the graphene surface.

The C_{EDL} was calculated in the MD simulations by computing the effective charge density of the solid surface (Q) and the potential difference (V) between the surface and the bulk solution.

V was obtained by solving the one-dimensional Poisson equation perpendicular to the graphene surface. The effective Q of the substrate at the point of zero charge was calculated from $\int_0^a F\left([K^+](z) - [Cl^-](z)\right) dz$, where F, z and a are the Faraday constant, the distance from graphene, and the smallest z when the charge is screened, respectively.

Raman Spectroscopy Characterizations

To rule out any effect of damage and degradation of graphene on transconductance levels, we performed Raman spectroscopy characterizations of graphene on two representative substrates, PTFE, the most hydrophobic substrate, and SiO_2 the most hydrophilic substrate. Spectra were taken at ten different points with equal spacing along the width of the graphene channel to demonstrate the consistent quality of the transferred graphene. Laser wavelength was 633 nm. As evidenced in the Raman spectra shown in Figure S11, the constant amplitude of the D-band of graphene (~1,350 cm^{-1}) for both indicates there is no significant difference in the quality of graphene between graphene/PTFE samples (Figure S11a) and graphene/SiO_2 samples (Figure S11b). These results, along with the similar two-terminal resistance levels for all samples (i.e., similar I_d levels at V_{CNP} in Figure 4a), suggest the conclusion that the suppressed transconductance level of graphene on hydrophobic substrates did not result from damage on graphene but is mainly attributed to the decrease in C_{EDL}.

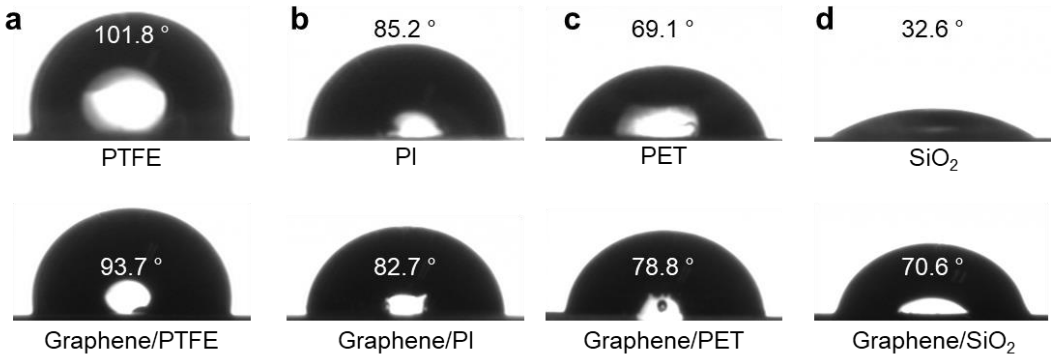

Figure S1. Goniometry WCA characterizations of the four bare substrates (top panels) and graphene/substrates (bottom panels).

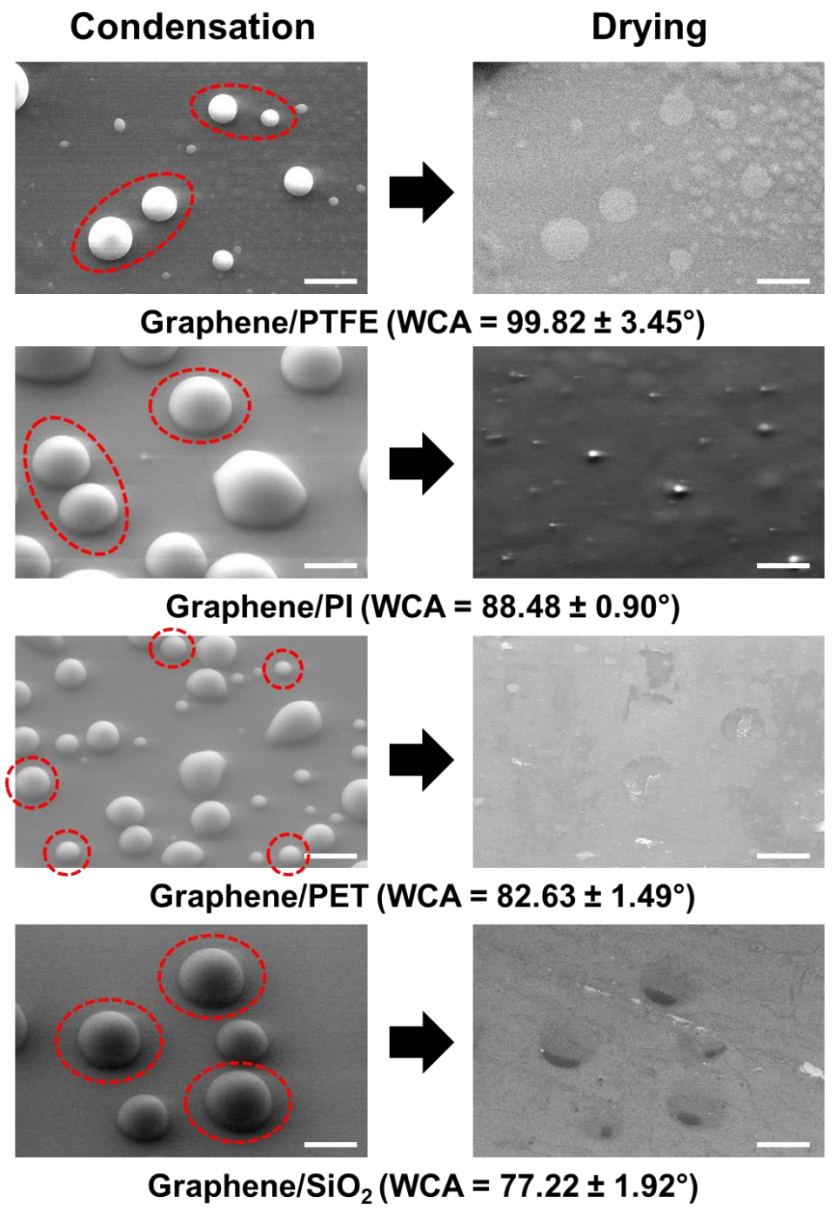

Figure S2. E-SEM WCA characterizations of the four graphene/substrates. The WCA calculations were performed only when no delamination/damage of graphene was observed after drying. In addition, only hemispheric water droplets were used for the calculation. The WCAs that were measured and calculated by E-SEM were 5-10° higher than those measured by goniometry due to the reduced gravitational effect on smaller droplets and the continuous growth of water droplets in E-SEM condensation mode[15].

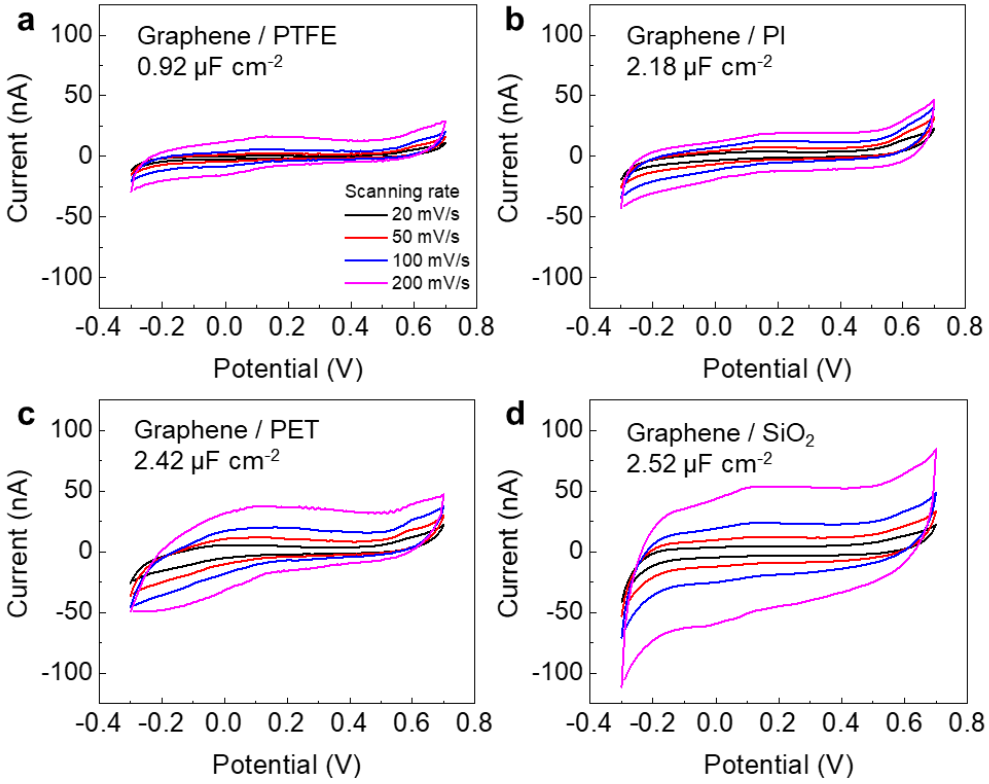

Figure S3. CV measurement results of the four graphene/substrates samples. Various sweep rates (from 20 to 200 mV/s) were used to ensure the reliability of the measurements. The curves at each sweep rate were obtained on the fifth cycle.

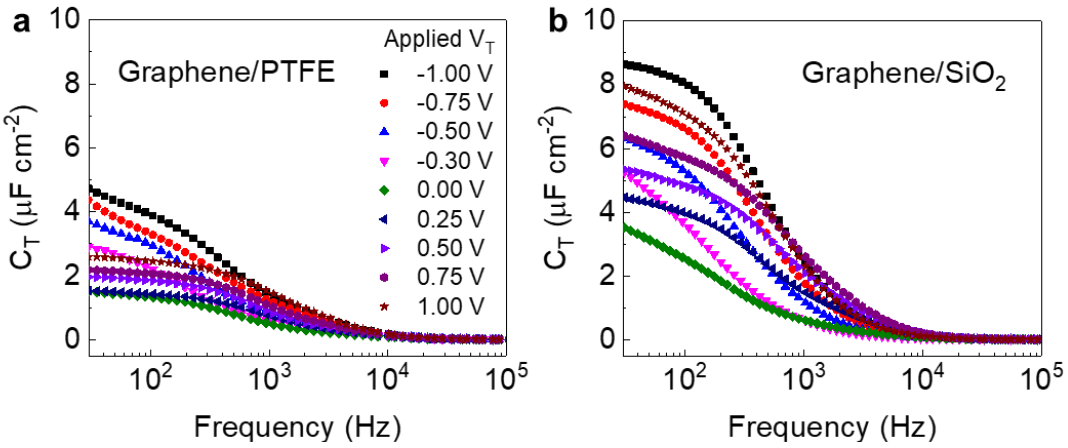

Figure S4. C_T – *log (f)* curves of (a) graphene/PTFE and (b) graphene/SiO_2 extracted from EIS at various gate voltages.

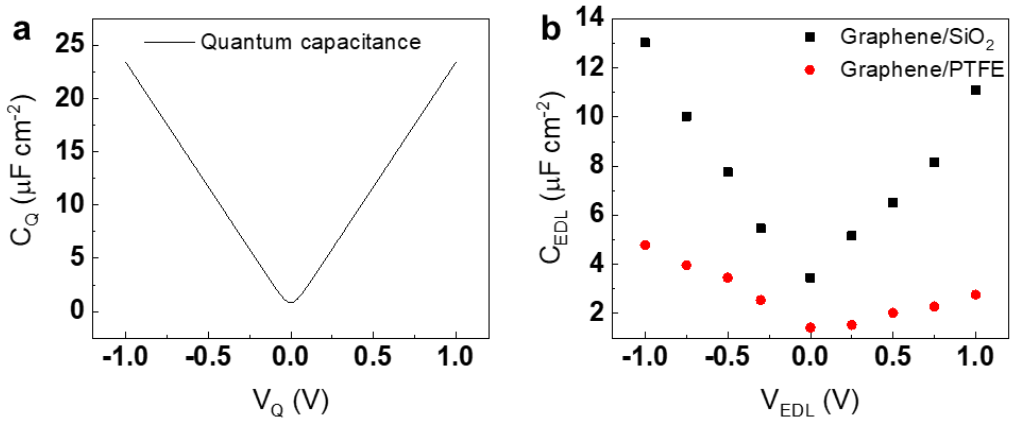

Figure S5. (a) Calculated C_Q of graphene, and (b) C_{EDL} extracted by subtracting C_Q (a) from the C_T (Figure 2d).

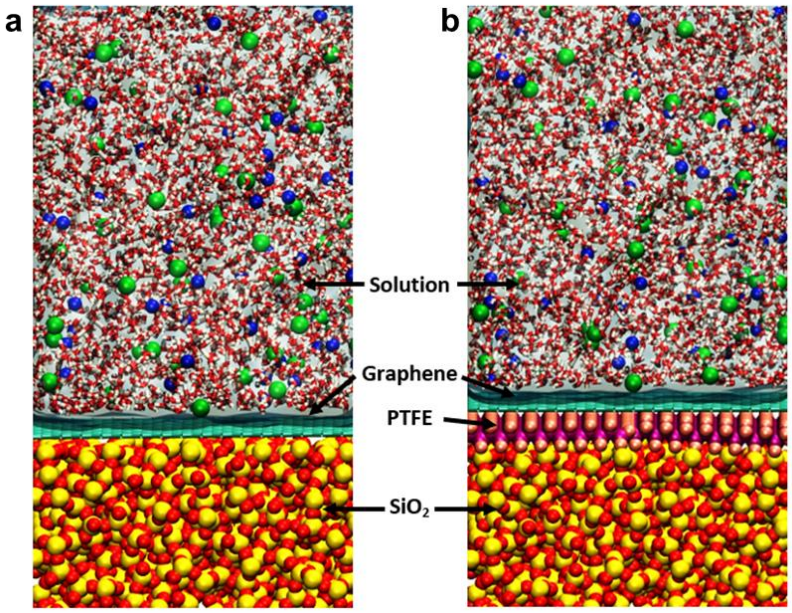

Figure S6. MD simulation setup for the electrolyte solutions (K^+ and Cl^- are presented by blue and green spheres, respectively) (a) near graphene (cyan) supported by SiO_2 substrate (Si and O atoms are presented in yellow and red, respectively) and (b) PTFE-coated SiO_2 substrate (C and F atoms are shown in purple and pink, respectively).

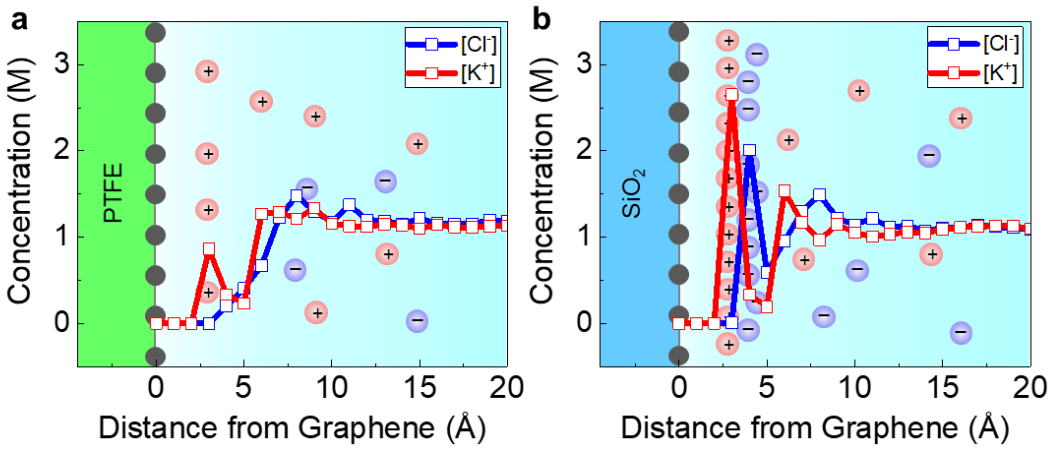

Figure S7. MD simulations of ion concentrations on (a) a graphene/PTFE and (b) a graphene/SiO_2 as a function of distance.

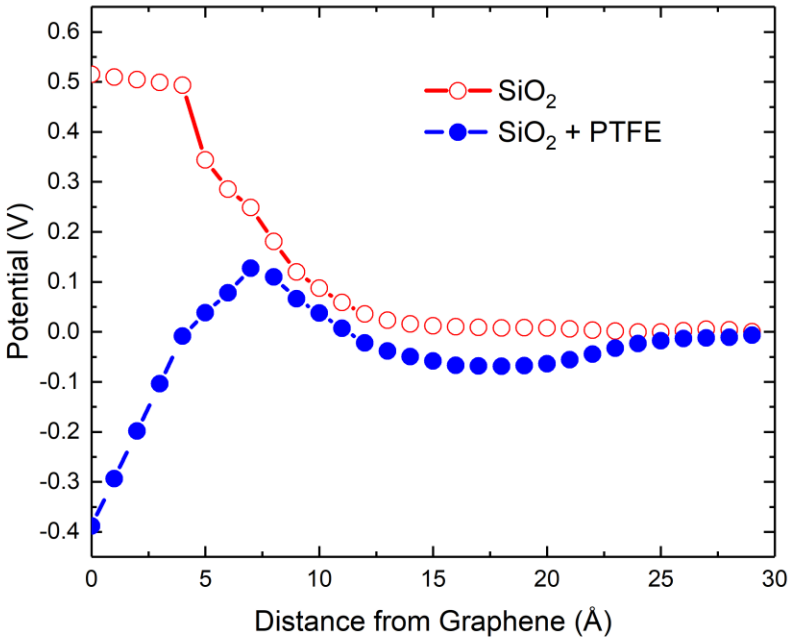

Figure S8. The electric potential as a function of distance from graphene (z) for both graphene/PTFE and graphene/SiO_2. The potential was obtained from $V(z) = -\iint_{z_0}^{z} \frac{q(z)}{A\,\varepsilon_0} dz\,dz$, where *q(z)*, *A* and ε_0 are the net charge of the ions in *z*, the surface area of graphene and the vacuum dielectric constant, respectively.

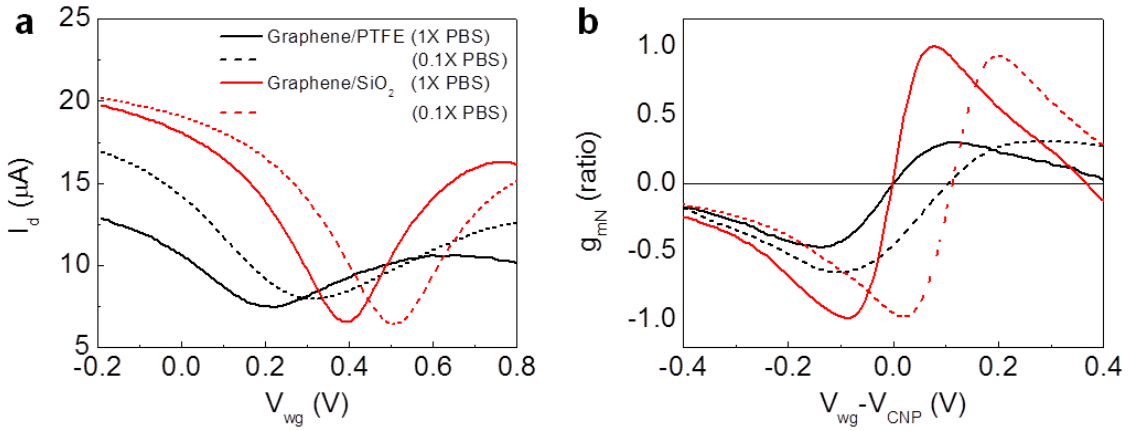

Figure S9. (a) Solution-gated I_d-V_{wg} charge transport characteristics of graphene FETs on PTFE (black) and SiO_2 (red) substrates with two different electrolyte concentrations. (b) Comparison of transconductance ratio based on the results shown in (a). 1X PBS (solid line) and 0.1X PBS (dashed line) solutions were used to investigate effects of ionic concentration.

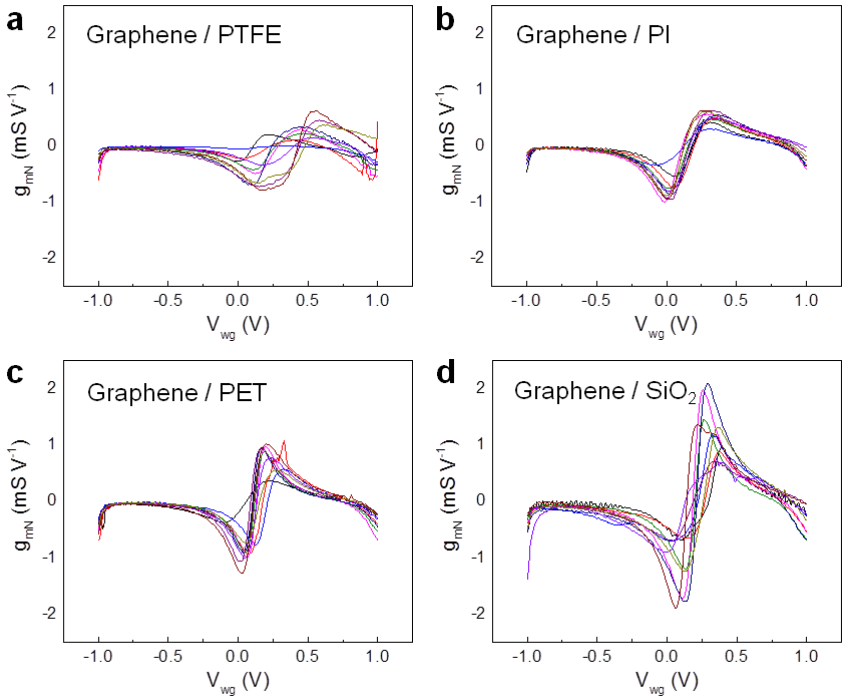

Figure S10. Transconductance levels from ten samples on each substrate.

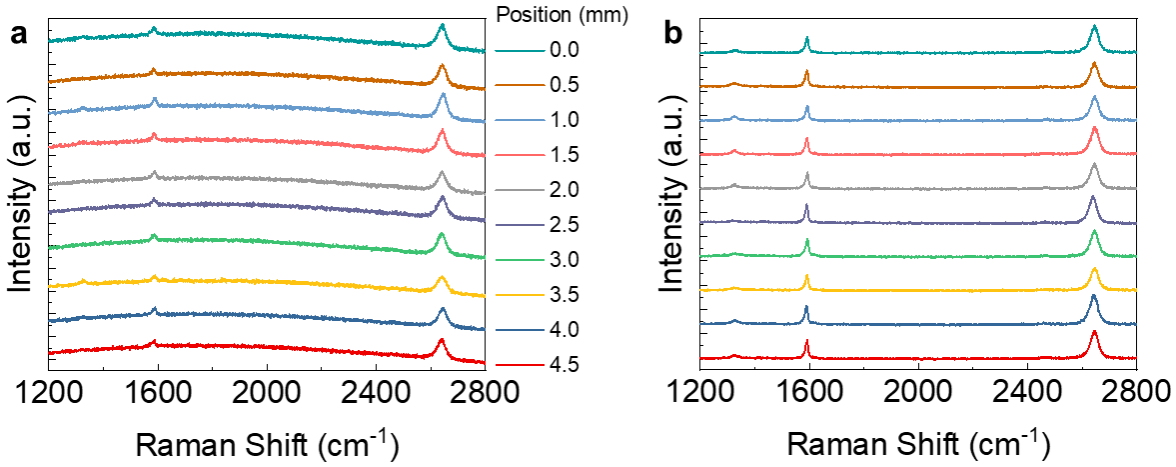

Figure S11. Raman spectra of graphene on the two representative substrates: (a) polytetrafluoroethylene (PTFE) and (b) SiO_2. A 633 nm laser was used on a Renishaw microPL/Raman microscope system. Ten measurement points were chosen along the width of the channels in 0.5 mm intervals between points. The Raman spectra from the ten measurement show minimal differences, supporting the consistent quality of transferred graphene.

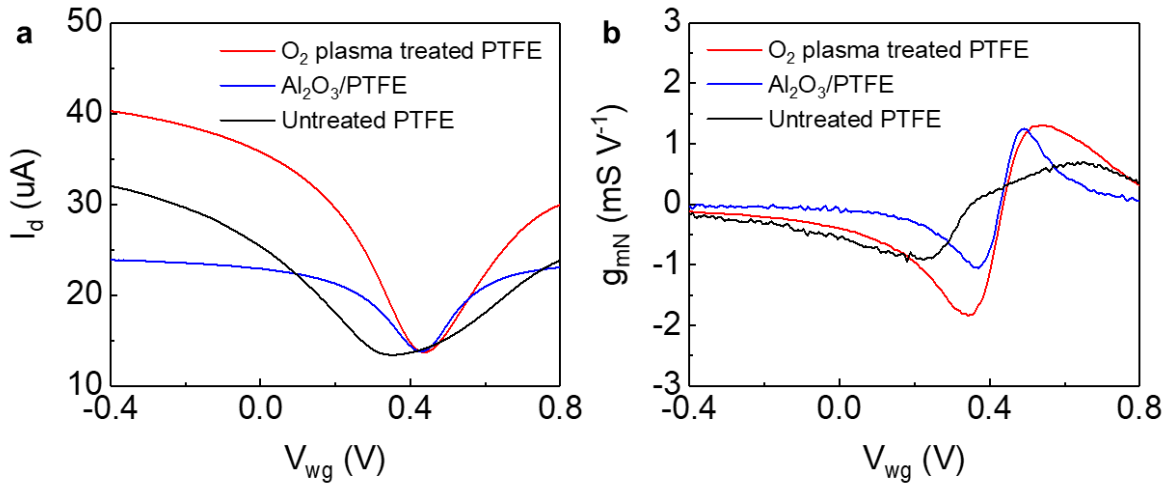

Figure S12. Comparison of the charge transport characteristics of graphene on O_2 plasma treated and Al_2O_3 coated, and untreated PTFE.

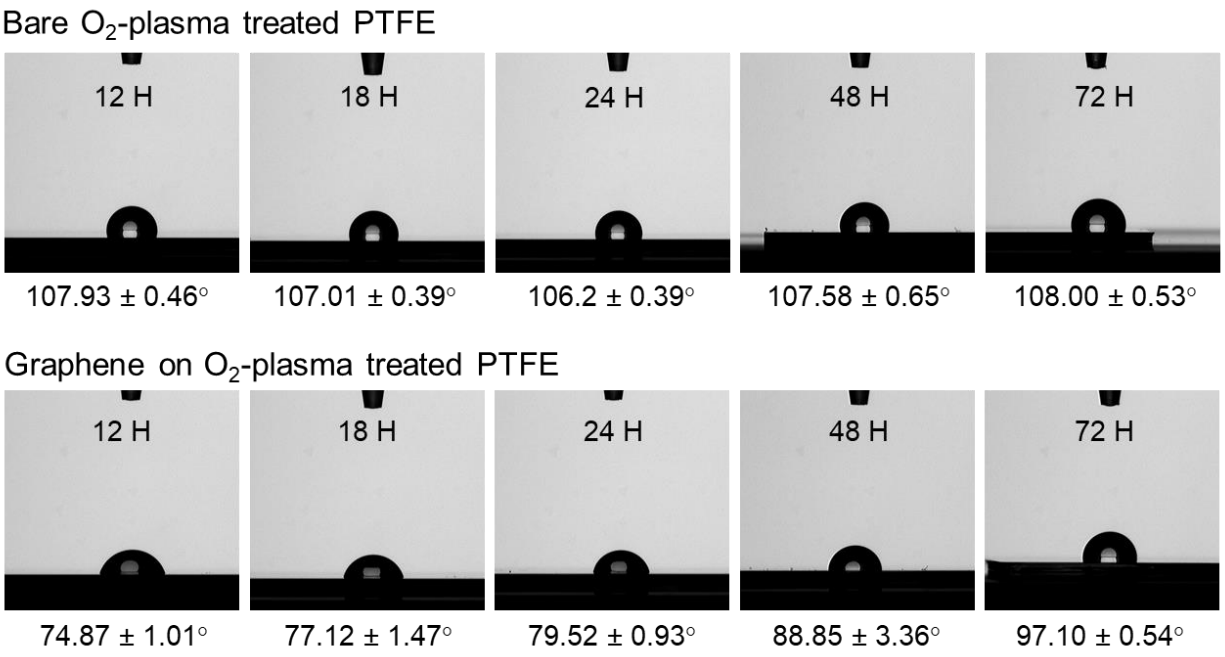

Figure S13. Time-dependent WCA change of graphene on O_2 plasma treated PTFE. The times shown in the figures are the times after O_2 plasma treatment.

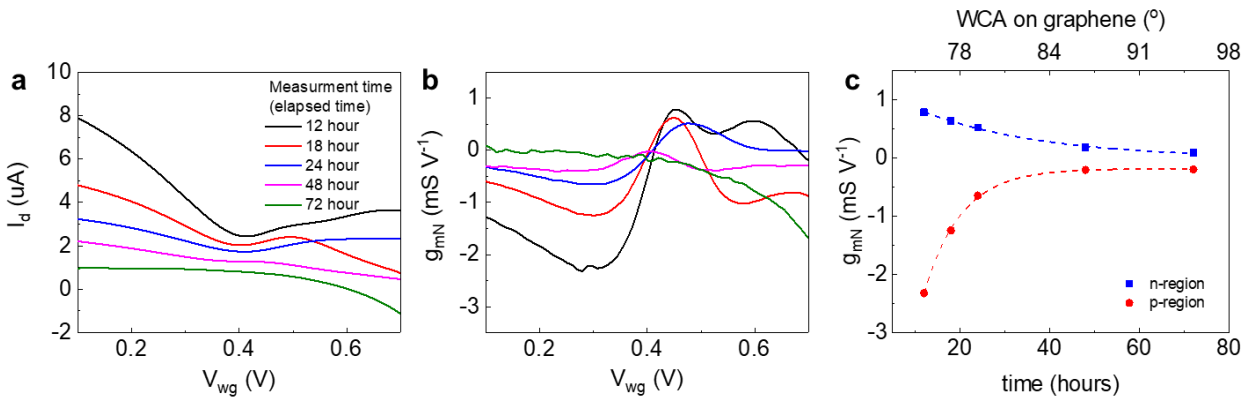

Figure S14. Aging effects on graphene on O_2 plasma treated PTFE. (a) I_d-V_{wg} Charge transport characteristics of a graphene FET on O_2 plasma treated PTFE as a function of aging time. We observed that a long aging time, particularly in the case of 72 hours aging, has led to the increased gate leakage current (Figure S15), possibly due to the increased hydrophobicity and contamination, and consequently the negative current in Figure S14a. (b) Calculated transconductance from (a) showing decreases in transconductance as the O_2 plasma treated substrate recovers hydrophobicity due to aging. (c) Plot of time-dependent WCA and transconductance change.

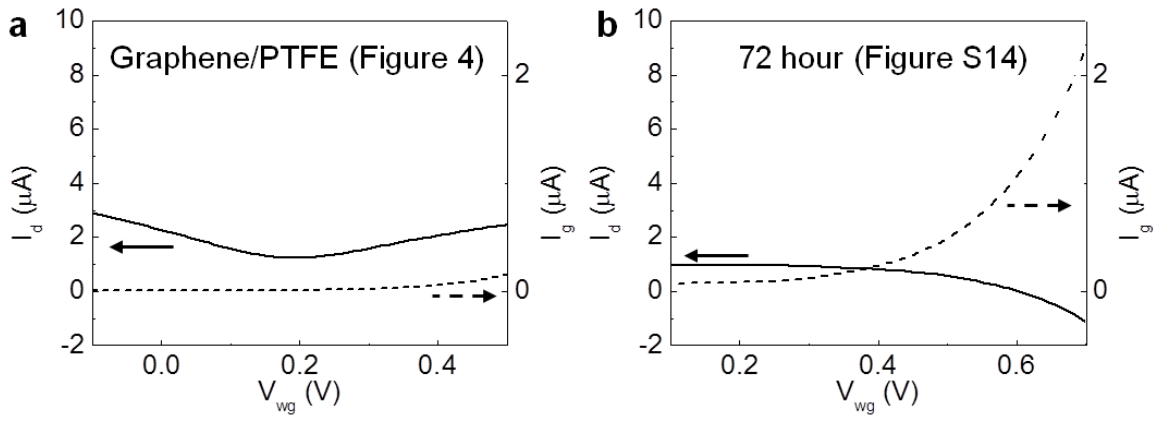

Figure S15. Gate leakage current data for (a) Figure 4a and (b) Figure S14a. Solid and dashed lines represent the I_d-V_{wg} characteristic curves and gate currents, respectively.

g_{mN} (mS V^{-1})	p-type	n-type
Graphene/SiO_2	-1.15±0.469	1.26±0.454
Graphene/PET	-0.903±0.226	0.809±0.224
Graphene/PI	-0.786±0.194	0.522±0.086
Graphene/PTFE	-0.471±0.233	0.227±0.149

Table S1. Average ± one standard deviation of the transconductance levels for each case.

	Modulation of C_T		Transconductance	
	V_T < 0 (-0.5 ~ 0)	V_T > 0 (0 ~ 0.5)	p-type	n-type
Graphene/SiO_2	-2.816 uF/(cm^2·V)	2.080 uF/(cm^2·V)	-1.28 mS/V	1.55 mS/V
Graphene/PTFE	-1.664 uF/(cm^2·V)	0.515 uF/(cm^2·V)	-0.71 mS/V	0.50 mS/V

Table S2. Comparison between the modulation level of C_T and the transconductance (i.e., current modulation level) for the two representative samples, Graphene/SiO_2 and Graphene/PTFE.

References

1. Schneider, C. A.; Rasband, W. S.; Eliceiri, K. W. *Nat. Methods* **2012**, *9*, 671–675.
2. Stalder, A. F.; Melchior, T.; Müller, M.; Sage, D.; Blu, T.; Unser, M. *Colloids Surfaces A Physicochem. Eng. Asp.* **2010**, *364*, 72–81.
3. Ashraf, A.; Wu, Y.; Wang, M. C.; Yong, K.; Sun, T.; Jing, Y.; Haasch, R. T.; Aluru, N. R.; Nam, S. *Nano Lett.* **2016**, *16*, 4708–4712.
4. Xia, J.; Chen, F.; Li, J.; Tao, N. *Nat. Nanotechnol.* **2009**, *4*, 505–509.
5. Fang, T.; Konar, A.; Xing, H.; Jena, D. *Appl. Phys. Lett.* **2007**, *91*, 092109.
6. Plimpton, S. *J. Comput. Phys.* **1995**, *117*, 1–19.
7. Humphrey, W.; Dalke, A.; Schulten, K. *J. Mol. Graph.* **1996**, *14*, 33–38.
8. Buneman, O. *SIAM Rev.* **1983**, *25*, 425–426.
9. Joung, I. S.; Cheatham, T. E. *J. Phys. Chem. B* **2008**, *112*, 9020–9041.
10. Wu, Y.; Aluru, N. R. *J. Phys. Chem. B* **2013**, *117*, 8802–8813.
11. Cygan, R. T.; Liang, J.-J.; Kalinichev, A. G. *J. Phys. Chem. B* **2004**, *108*, 1255–1266.
12. Daly, K. B.; Benziger, J. B.; Debenedetti, P. G.; Panagiotopoulos, A. Z. *J. Phys. Chem. B* **2013**, *117*, 12649–12660.
13. Nosé, S. *J. Chem. Phys.* **1984**, *81*, 511–519.
14. Hoover, W. G. *Phys. Rev. A* **1985**, *31*, 1695–1697.
15. Choi, J.; Mun, J.; Wang, M. C.; Ashraf, A.; Kang, S.-W.; Nam, S. *Nano Lett.* **2017**, *17*, 1756–1761.